Prognosis of wear progression in electrical brakes for aeronautical applications

Andrea De Martin[1], Giovanni Jacazio[2], Vincenzo Parisi[3] and Massimo Sorli[4]

[1,2,3,4]*Politecnico di Torino, Department of Mechanical and Aerospace Engineering, Torino, 10129, Italy*

andrea.demartin@polito.it
giovanni.jacazio@formerfaculty.polito.it
vincenzo.parisi@studenti.polito.it
massimo.sorli@polito.it

ABSTRACT

The evolution towards "more electric" aircrafts has seen a decisive push in the last decade, due to the growing environmental concerns and the development of new market segments (flying taxis). Such push interested both the propulsion components and the aircraft systems, with the latter seeing a progressive trend in replacing the traditional solutions based on hydraulic power with electrical or electro-mechanical devices. Although more attention is usually devised towards the flight control actuation, an interesting and fast-developing application field for electro-mechanical systems is that of the aeronautical brakes. Electro-mechanical brakes, or E-Brakes hereby onwards, would present several advantages over their hydraulic counterparts, mainly related to the avoidance of leakage issues and the simplification of the system architecture. The more difficult heat dissipation, associated with the thermal issues that usually constitute one of the most significant sizing constraints for electro-mechanical actuators, limits so far, their application (or proposal of application) to light-weight vehicles. Within this context, the development of PHM solutions would align with the need for an on-line monitoring of a relatively unproven component. This paper deals with the preliminary stages of the development of such PHM system for an E-Brake to be employed on a future executive class aircraft, where the brake is actuated through four electro-mechanical actuators. Since literature on fault diagnosis and prognosis for electrical motors is fairly extensive, we focused this preliminary analysis on the development of PHM techniques suitable to monitor and prognose the evolution of the brake pads wear instead. The paper opens detailing the system architecture and continues presenting the high-fidelity dynamic model used to build synthetic data-sets representative of the possible operating conditions faced by the E-Brake within realistic operative scenarios. Such data are then used to foster a preliminary feature selection process, where physics-based indexes are compared and evaluated. Simulated degradation histories are then used to test the application of data-driven fault detection algorithm and the possible application of particle-filtering routines for prognosis.

1. INTRODUCTION

Despite being a rather recent subject, the development of E-Brake systems is a critical step towards the complete electrification of aircraft systems. Given their relatively unproven technology, the definition of a comprehensive PHM system would provide additional confidence towards their application, lowering the risk of unanticipated failures, reducing the aircraft downtimes and giving access to strategic information useful to optimize the fleet management. Although literature on PHM activities for the most common components of electro-mechanical brakes is extensive, few papers have been published about the E-Brakes themselves. In (Ramesh et al. 2021) authors propose a FDI algorithm to observe and correctly assess the most probable failures occurring in a simple electro-mechanical brake for aeronautic applications. The analysis considers an aeronautical brake actuated by one Electro-mechanical actuator driven through a brushed DC-motor and is mainly focused on electrical failures. In (Oikonomou et al. 2022) authors investigate the prognosis of wear in aeronautical brakes through the analysis of historical series of brake pads thickness. Data-driven techniques are applied to perform the long-term prognosis, and the results of an interesting benchmarking activities comparing the performances of several algorithms are provided. Results are promising but assume the presence of dedicated sensors to measure the thickness of the brake pads, which are not foreseen for the application under study in this paper. The E-LISA research project, under way within the Clean Sky 2/Clean Aviation framework, has the objective of developing an innovative iron bird dedicated to executing tests on the landing gear of a small aircraft equipped with an electro-mechanical landing gear and electrical brake. The E-

LISA iron bird consists of a multi-functional intelligent test facility integrating hardware and software, allowing all the tests and analyses perceived as fundamental to be performed to demonstrate the maturity of an electro-mechanical landing gear, hence paving the way for its implementation in a small passenger aircraft and will include prognostics and health management (PHM) functionalities for the electrical brake system. Such tests include the simulation of complete landing procedures under different operating conditions such as runway friction (wet/dry), presence of waving and irregularities along the runway, variable aircraft weight, and approach speed as detailed in (De Martin et al. 2022). This paper deals with the preliminary analysis needed to develop a comprehensive PHM system for the E-Brake, focusing on the feature selection, fault detection and prognosis of wear in the brake pads without the addition of dedicated sensors considering the case study of a real E-Brake system, currently under development. To meet such objective authors resorted to the definition of a high-fidelity simulation environment able to represent the expected behavior of the electrical brake under variable operating conditions and dynamically evolving wear conditions, mirroring the approach already applied to primary flight control actuators in (Autin et al. 2021). The paper is organized as follows. At first the case study under consideration is presented in detail, highlighting its most prominent characteristics and their expected effect on the definition of the prognostic system. The operational scenario considered for the E-Brake at hand is also introduced and discussed. The paper focus is then shifted to the high-fidelity simulation model and the definition of a suitable degradation model to replicate the effects of wear progression on the brake behavior. Simulation results are then used to pursue the feature selection process and used to foster the definition of a fault detection/failure prognosis framework based upon a combination of data-driven and particle filtering techniques. Such algorithms are then applied to the most suitable feature candidates and their results compared.

2. CASE STUDY AND OPERATIONAL SCENARIO

The case study under analysis is an E-Brake system for an executive-class aircraft with an expected weight at take-off of around 6 tons. Two E-Brake systems are integral with the Main Landing Gear system, one for the Left-Hand side, one for the Right-Side each. As depicted in Figure 1, each E-Brake is a multi-disk assembly actuated through four Electro-Mechanical Actuators (EMAs) controlled in force. Whenever the pilot acts on the brake pedals, a force command is sent towards the E-Brake system; such command signal is processed by the Brakes Control Unit (BCU), which can cut the force command signal through the touch-down protection routines, avoiding that the brakes are actuated before the aircraft rotation during landing has ended. The command signal can be further modulated by the electronic anti-skid system, which decreases the force request depending on the runway conditions to avoid the occurrence of wheel blockage events and excessive slip according to a combination of pilot input and automatic recognition of the runway status.

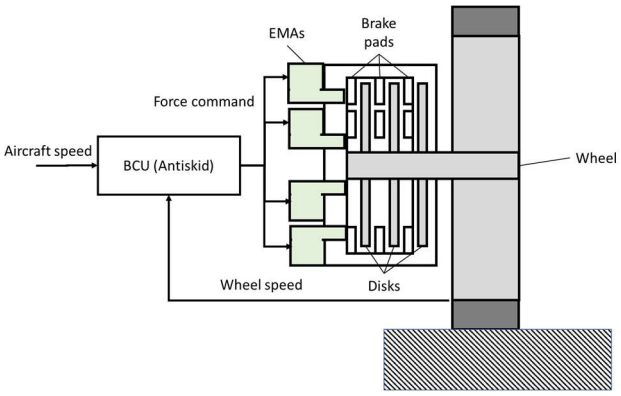

Figure 1. Case-study architecture.

The electro-mechanical actuators, which schematics is provided in Figure 2, are driven by one Brushless-DC motor with each, and act on the brake pads through a mechanical transmission made of a one-stage reducer and a ball-screw. Each actuator is equipped with a force sensor to measure the exerted action, while a resolver integral with the motor shaft is used to infer its position and realize the Field Oriented Control of its phase currents. The PHM system considered for this research activity is projected to work at the Landing Gear System level, thus having access to all the signals available within the Landing Gear control system, including:

- E-Brake motors phase currents
- Angular position of the E-Brake motors shaft
- Pilot command

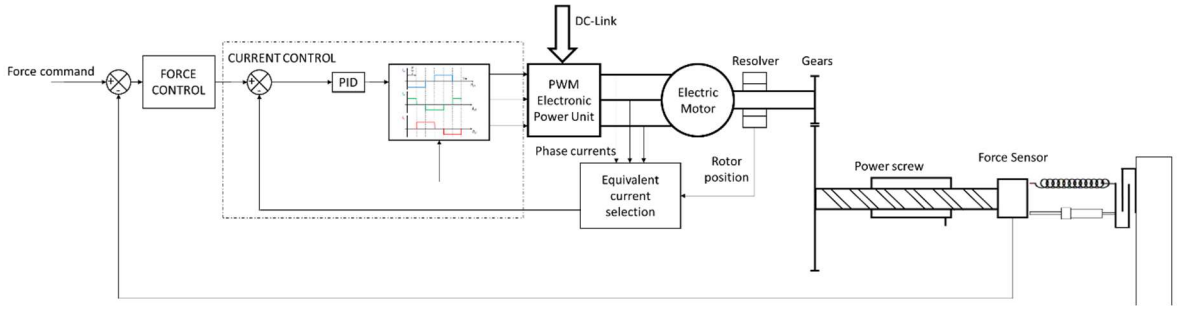

Figure 2. The E-Brake actuators.

- Anti-skid and touch-down protection signals
- Exerted force measurement for each EMA

To complete the description of the case study under analysis it is also critical to introduce the operational scenario faced by the landing gear system during its projected functional life. Such operation is important both to properly characterize the expected behavior of the E-Brake system under nominal health status, but also to anticipate the effects that significant variations in the operational conditions may have on the E-Brake signals and thus on the possible feature candidates. Starting with the operating temperature, the E-Brake system is expected to operate in presence of external temperatures ranging from -40°C to + 60°C in combination with variable runway conditions (dry, wet, snowy, with ice). Moreover, a variation of $\pm$ 10% of the average weight at landing can be expected as a function of the fuel consumption and passengers' number. The same percentual variation is also applied on top of the nominal aircraft horizontal speed during the final approach (50 m/s).

3. SIMULATION MODEL

To replicate the Landing Gear system behavior, we resort to the high-fidelity model provided in (De Martin et al. 2022), capable of representing the entire landing procedure under the assumption of symmetric touch-down, thus with null roll angle and equal weight repartition between the two main landing gear legs. In such model the aircraft is represented as a rigid body subjected to the aerodynamic components of Lift due to the aircraft wing (L), anterior wing (Lfw), tail wing (Lt), and Drag (D). Each of these components is expressed as a function of the attack angle of the related aerodynamic surface and scales with the square of the wind speed. Making reference to Figure 3, the vertical, horizontal and pitch dynamics of the vehicle can then be represented as a system of three differential equations.

$$\begin{cases} -2F_{MLG} - F_{NLG} - W + L\,c\vartheta + L_t c\vartheta + L_{fw} c\vartheta + Ts\vartheta - Ds\vartheta = m_{air}\ddot{z} \\ 2\,F_{MLG,i} H_{MLG} - L\,H_L - L_T\,H_{Lt} + L_{fw} H_{Lfw} - F_{NLG} H_{NLG} = I_{yy}\ddot{\vartheta} \\ Tc\vartheta - \sum_i F_{t,i} = m_{tot}\ddot{x} \end{cases} \quad (1)$$

where $c\vartheta = cos\vartheta$ and $s\vartheta = sin\vartheta$. T is the motors thrust, while F_{MLG}, F_{NLG} and $F_{t,i}$, are respectively the force exerted on the aircraft by the Main Landing Gears, the Nose Landing Gear and the friction forces between the aircraft tires and the runway (Cook 2012). The main inertia moment I_{yy} and the position of the center of mass of the aircraft (thus the torque lever arms $H_D, H_L, H_{L_t} \ldots$) are variable according to data provided by the industrial partners of the project as a function of the aircraft acceleration and attitude. The total mass of the aircraft is addressed as m_{tot} equal to the sum of the aircraft mass (m_{air}) and the overall mass of the main and nose landing gears.

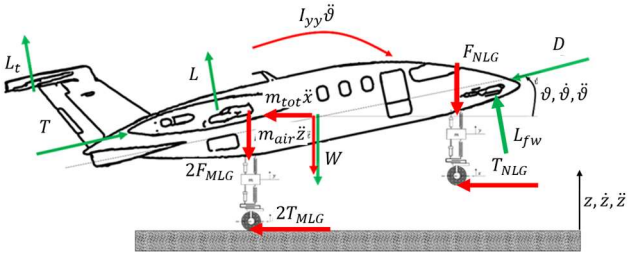

Figure 3. Aircraft dynamic equilibrium.

Each landing gear leg is described as a two-degrees-of-freedom system as shown in Figure 4. The shock absorber characteristics are known and provided by the landing gear supplier. Similarly, the vertical dynamics of the leg can be represented as a function of the stiffness (k_t) and damping (c_t) coefficient representative of the contact between tire and runway, while x_w and x_{rw} are respectively the vertical displacement of the wheel and that of the runway simulator, by default equal to zero. The wheel mass is m_w, while m_{leg} is the mass of the leg. The characteristics of the tire are derived from data provided by the industrial partners.

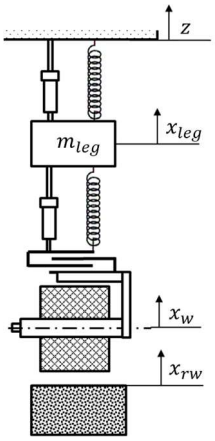

Figure 4. Landing Gear leg model.

The rotational dynamics of the wheel can be described according to the free-body diagram of Figure 5. We address with $F_n = k_t(x_w - x_{rw}) + c_t(\dot{x}_w - \dot{x}_{rw})$ the vertical force exchanged between the wheel and the runway and with $F_t = F_n\mu$ the friction force. u_{rw} is the rolling friction parameter, expressed as a function of the wheel angular frequency and of the tire pressure (Carbone and Putignano 2013).

$$F_n\mu\left[\frac{D_w}{2} - (x_{leg} - x_{rw})\right]\text{sign}(\lambda) - F_n u \tanh\dot{\vartheta}_w - c_w\dot{\vartheta}_w - T_{brk} = I_w\ddot{\vartheta}_w \quad (2)$$

where ϑ_w is the wheel rotation, I_w is the moment of inertia of the wheel assembly, D_w its diameter and c_w the viscous friction coefficient roughly representative of the dissipation in the wheel supports. The friction coefficient μ is evaluated according to the Burckhardt model (M. Burckhardt 1993) as

a function of the slip factor λ between wheel and runway simulator.

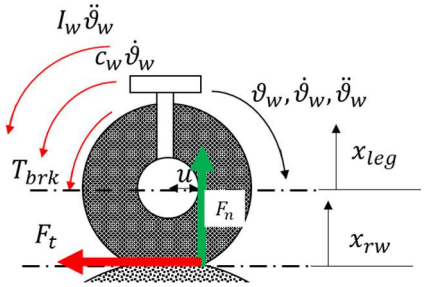

Figure 5. Aircraft dynamic equilibrium.

The E-Brake system is made of four Electro-Mechanical Actuators (EMAs) controlled in force and acting in parallel on a disk brake. The EMAs model is derived from the dynamic representation of similar systems employed as flight control actuators (De Martin et al. 2017). The control system is described as a two-nested control loops, where a sequence of Proportional-Integrative controllers operates on the force control loop and on the current control loop of each brushless motor. The sensors are modelled through second order transfer functions replicating the expected dynamics of the load cell and of the Hall-effect sensors employed to monitor the angular position of the Brushless-DC rotor. The simulation of the measure chain is complete with the model of the employed A/D converters. The dynamic model of each EMA features a functional description of the Electronic Power Converter derived from (Mohan et al. 2005) for a three-phase inverter controlled through Pulse Width Modulation (PWM). The electrical dynamics of the motor is described according to a streamlined three-phase model of the system, where $V_{a,b,c}$ and $i_{a,b,c}$ are the phase voltages and currents.

$$[V_{a,b,c}] = [\boldsymbol{R_{a,b,c}}(T_w)][i_{a,b,c}] + [\boldsymbol{L}(T_w)]\frac{d}{dt}[i_{a,b,c}] + \frac{d}{dt}[\phi_{a,b,c}(\vartheta_{el})] \quad (3)$$

$[\mathbf{R_{a,b,c}}]$ is the electric resistance matrix, which elements depends on the windings' temperature (T_w). [**L**] is the inductance matrix, accounting for self-induction and mutual induction phenomena along with the effect of magnetic flux dispersion. Finally, $[\phi_{a,b,c}]$ is the concatenated magnetic flux provided by the permanent magnets, function of the electrical angle (ϑ_{el}). The torque at the motor shaft can then be computed, leading to the the dynamic equilibrium of the rotor

$$\sum_{a,b,c}\frac{d\phi}{dt}i_{a,b,c} - c\dot{\vartheta}_m - k_m(\vartheta_m - \vartheta_{gb}) - c_m(\dot{\vartheta}_m - \dot{\vartheta}_{gb}) = I_m\ddot{\vartheta}_m \quad (4)$$

where ϑ_m and ϑ_{gb} are the angular position of the motor shaft and of the gears. I_m is the moment of inertia of the rotor, while k_m and c_m address the torsional stiffness of the motor shaft and its associated damping. The gear pair is described as a rotational mass-spring-damper system, thus leading to the following equation,

$$k_m(\vartheta_m - \vartheta_{gb}) + c_m(\dot{\vartheta}_m - \dot{\vartheta}_{gb}) - \frac{1}{\tau}[k_{gb}(\vartheta_{gb} - \vartheta_{rs}) + c_{gb}(\dot{\vartheta}_{gb} - \dot{\vartheta}_{rs})] - T_{fr,gb} = I_{gb}\ddot{\vartheta}_{gb} \quad (5)$$

where τ is the transmission ratio, $T_{fr,gb}$ the friction torque, while ϑ_{rs} is the angular position of the rotating part of the screw. The friction torque is computed as the sum of three components, one dependent on the acting load, one related to the viscous friction and a drag torque component. The power-screw is modelled as a two-degrees of freedom elements, where the rotating part is connected to the translating element through a viscoelastic element. Defining with $x_{rs,i}$ the position of the translating portion of the screw pertaining to the i-th actuator, it becomes possible to describe the brake dynamics, and thus that of the pads. Addressing with k_{eb} the stiffness, it is possible to evaluate the braking torque acting on the landing gear wheel as a function of the translating mass of the brake pads m_{eb}, its translation x_{eb} and the angular speed of the wheel $\dot{\vartheta}_w$ as,

$$\begin{cases} T_{brk} = 0 \ \leftrightarrow x_{eb} < x_{thr} \\ T_{brk} = f_{eb}[k_{eb}(x_{eb} - x_{thr}) - c_{eb}(\dot{x}_{eb})] \ \leftrightarrow x_{eb} \geq x_{thr} \end{cases} \quad (6)$$

where $f_{eb} = f_{eb}(\dot{\vartheta}_w)$ is the friction coefficient between the brake pads and disk, function of the wheel angular frequency. Knowing the braking torque and the wheel angular frequency it is possible to compute the mechanical power transformed into heat by the braking process. Such power is used within a simplified thermal model of the E-Brake assembly to estimate at each time step the temperature of the pads and the temperature of the electric motor windings considering both the thermal power generated by the motor themselves and that transmitted to the external environment. Since the pads contact the brake disks only when their translation x_{eb} overcomes a predefined stroke equal to x_{thr}, it is possible to model the effects of the pads wear by properly increasing such threshold value under the assumption that the brake pads return in the original position once the braking procedure is finished. According to (Olesiak et al. 1997; Yevtushenko et al. 2017) , wear progression in brake pads can be described as dependent on an experimental coefficient f_{wear} and k_{wear}, function of the local absolute temperature T, the sliding velocity between disks and pads v, and the contact pressure p.

$$\Delta x_{thr} = \int_t f_{wear}(T)K_{wear}(T)v(t)p(t)dt \quad (7)$$

Expressing the sliding velocity as a function of the wheel angular frequency $\dot{\vartheta}_w$ and the radial coordinate of the pads with respect to the wheel axis R_{pad}, we have

$$v = \dot{\vartheta}_w R_{pad} \tag{8}$$

The average pressure within the pads/disks contact area can be computed as a function of the braking force exerted by the four actuators and the pad contact area.

$$p = \frac{k_{eb}(x_{eb} - x_{thr}) - c_{eb}(\dot{x}_{eb})}{A_{pad}} \tag{9}$$

An example of the model behavior for different level of wear (no wear and critically advanced wear), is provided in Figure 6, where it is evident how the pads wear introduces an additional delay on the brake response due to the additional stroke required to cover the additional gap.

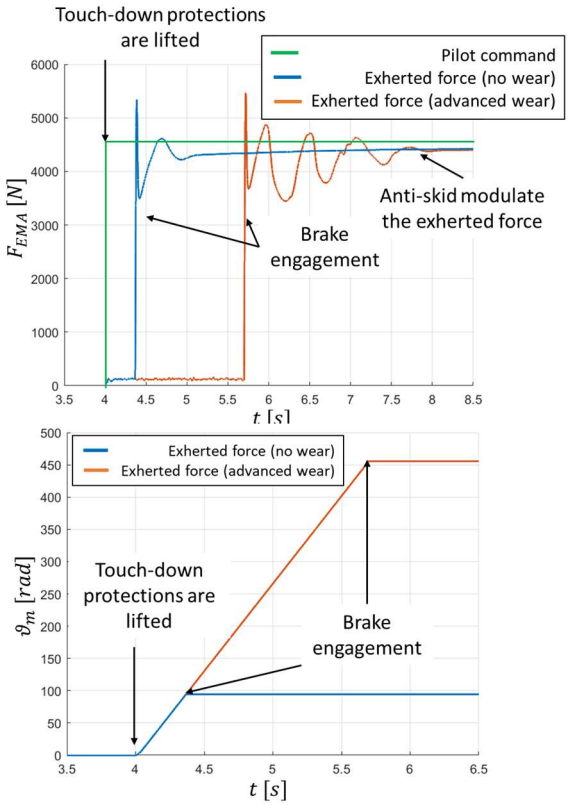

Figure 6. Model response in nominal and severely degraded conditions.

4. FEATURE SELECTION

The high-fidelity model was employed to build a preliminary database considering increasing levels of wear, varying the operating conditions (temperature, runway conditions, approach speed) as indicated in Section 3. Moreover, Gaussian noise was applied on the parameters of each of the four EMAs driving the E-Brake. The characteristics of such noise are dependent on the nature of the perturbated parameters and are meant to represent the effects of the expected production and design tolerances on the EMA behavior. As a consequence, the behavior of each EMA is slightly different from the others, even though the nominal value of the parameters used to model their dynamics is the same. Given the time-consuming nature of simulating an entire landing process, a total of thirty simulations for each considered wear level were performed. As anticipated in Section 3, the main macroscopic effect of the wear progression is in the increase of the free stroke that needs to be covered by the EMAs to get the pads in touch with the disks, leading to the progressive increase of the delay between the force command sent to the actuators and the actual generation of a braking torque. Considering this observation and given the signals considered available to the PHM system, a few feature candidates were isolated and evaluated according to correlation, accuracy, signal-to-noise ratio as advised by (Vachtsevanos et al. 2006). The most prominent feature candidates analyzed in this work are reported in Table 1 along with their performance indexes, while their behavior is summarized in Figure 7. Please notice that to avoid excessive clutter within the figure, the scatter plots report only the points correspondent to the average of the data distribution obtained for each considered level of wear. Moreover, features are reported as non-dimensional in order not to disclose sensible data on the E-Brake under examination. The first feature candidate, f_1, is computed as the delay between the time instant at which the motor shaft begins to move $t_{0,m}$ and the time instant for which the braking torque signal raises from zero $t_{0,f}$. Both time instants are isolated studying the moving variance of the motor shaft position signal and the braking force signal. The second feature candidate f_2 is instead computed as the angular rotation of the motor shaft $\Delta\vartheta_m$ between the time instants $t_{0,m}$ and $t_{0,f}$. Although these two candidates are expected to be correlated, they are expected to be affected differently from the variations in the operating conditions. The second feature is expected to be less influenced by the fluctuations in the mechanical efficiency of the EMA due to low temperatures or lubrication ageing, making it the preferrable choice between the two in the considered case. This second feature might be however not suitable if the resolution of the motor shaft position signal is lacking. The third considered feature candidate f_3 is the autocorrelation between the force signal measured during the braking procedure and a database of the expected braking force during landing.

Table 1. Feature candidates

Feature	Correlation	Accuracy	S/N Ratio
$f_1 = \Delta t$	0.98	0.98	7.65
$f_2 = \Delta\vartheta_m$	0.99	0.9	7.98
$f_3 = \rho(F_{EMA})$	0.96	0.75	3.65

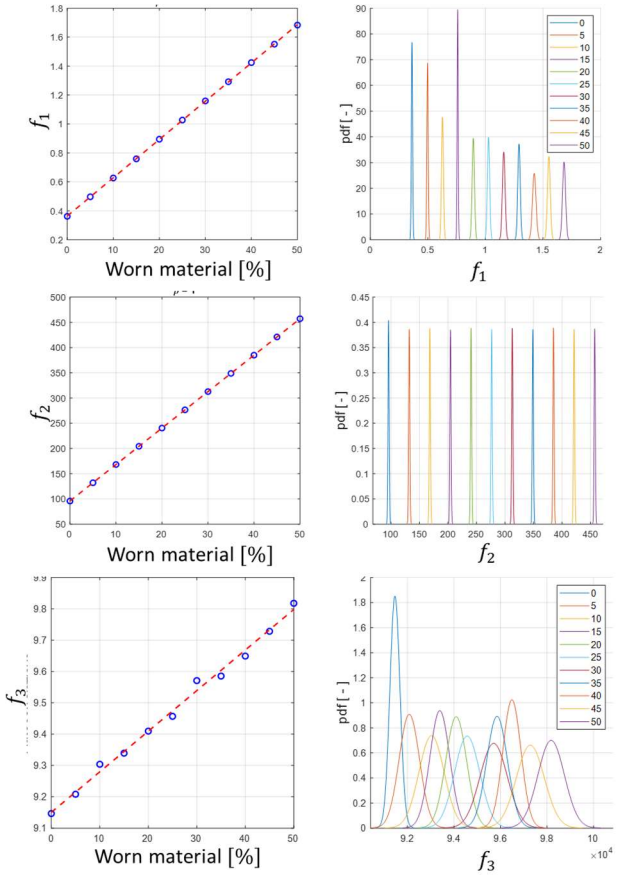

Figure 7. Feature candidates' behavior.

This feature provides interesting results and would be advantageous over the first two options since it does not require the knowledge of the angular position of the motor shaft. It is however expected that other failure modes, related to the motor electrical windings, can affect its behavior and has been as such discarded.

5. FAULT DETECTION

The chosen fault detection routine is based on a simple data-driven technique, where the running distributions of the selected features are compared against baselines representative of the nominal health behavior. In this scheme, the fault alarm is raised if the confidence level in the fault declaration overcomes a pre-defined threshold. According to (Vachtsevanos et al. 2006), such approach allows to adapt the baseline conditions to the peculiarities of each monitored subsystem, containing at the same time the computational effort required to process the signals coming from the field. To evaluate the behavior of the proposed routine and the performances of the proposed features, we simulated the possible life cycle of three E-Brake systems through the high-fidelity model presented in Section 3. The model was deployed to simulate a succession of landing in randomly varying operating conditions, computing at each time step the wear progression according to the model described by Equations (7-9). The tests were performed considering a confidence level threshold of 0.95. Example of the obtained results are reported in Figure 8, where the features distributions for healthy (in white), current (in yellow or grey) and at fault declaration (in red) conditions are depicted for each fault type. The system also provides in output the expected confidence associated with the fault declaration and the eventual presence of a fault alarm. The fault detection routine was able to successfully detect the early insurgence of brake pads wear in all the presented test cases. The average time at detection for the considered features is estimated in 186 landing events for f_2 and 386 landing events for f_1.

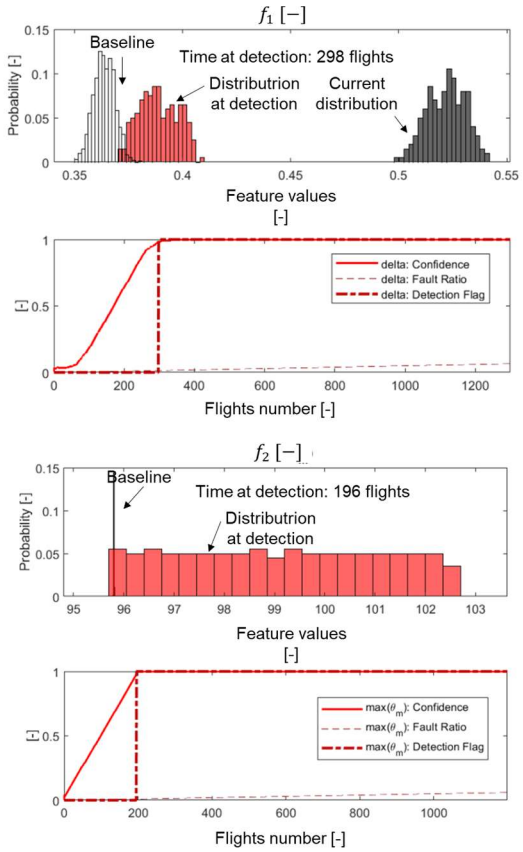

Figure 8. Examples of fault detection results for features f_1, f_2.

6. PROGNOSIS

Prognosis is achieved through a Bayesian estimation method using a particle filtering approach as firstly proposed by (Orchard and Vachtsevanos 2009). This method takes advantage of a nonlinear process (fault / degradation) model to describe the expected dynamics of the fault progression and a measure model derived from the feature/wear progression dependence observed during the feature selection phase. Prognosis through particle filtering is achieved by performing two sequential steps, prediction and filtering. Prediction uses both the knowledge of the previous state

estimate and the process model to generate the a priori estimate of the state probability density functions (pdfs) for the next time instant,

$$p(x_{0:t}|y_{1:t-1}) = \int p(x_t|y_{t-1})p(x_{0:t-1}|y_{1:t-1})\,dx_{0:t-1} \quad (10)$$

This expression usually does not have an analytical solution, requiring Sequential Monte Carlo algorithms to be solved in real-time with efficient sampling strategies (Roemer et al. 2011). Particle filtering approximates the state pdf using samples or "particles" having associated discrete probability masses (often called "weights") as,

$$p(x_t|y_{1:t}) \approx \tilde{w}_t(x_{0:t}^i)\delta(x_{0:t} - x_{0:t}^i)dx_{0:t-1} \quad (11)$$

where $x_{0:t}^i$ is the state trajectory and $y_{1:t}$ are the measurements up to time t. The simplest implementation of this algorithm, the Sequential Importance Re-sampling (SIR) particle filter (Arulampalam et al. 2009), updates the weights using the likelihood of y_t as:

$$w_t = w_{t-1}p(y_t|x_t) \quad (12)$$

Although this traditional particle filtering technique has limitations, in particular with regards to the description of the distributions tails, and more advanced resampling schemes have been proposed (Acuña and Orchard 2017), this technique was still deemed valid for a purely preliminary analysis. Long-term prediction of the fault evolution can be obtained by iterating the "prediction" stage, and are used to estimate the probability of failure in a system given a hazard zone that is defined via a probability density function with lower and upper bounds for the domain of the random variable, denoted as H_{lb} and H_{up}, respectively. Given the probability of failure, the RUL distribution for any given prediction can be computed along with the risk function (Acuña and Orchard 2018).

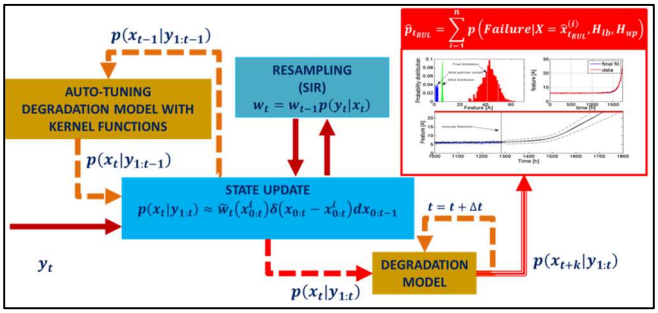

Figure 9. Prognostic routine.

The algorithm adopted for this paper follows the scheme provided in in Figure 9 (De Martin et al. 2018); this approach makes use of degradation models that are tuned or their parameters adjusted through Recursive Least Square (RLS) algorithm embedded in the main routine, to compute the current a priori state of the system, $p(x_t|y_{1:t-1})$, and to perform the iterative calculation that leads to the long term prediction $p(x_{t+k}|y_{1:t})$. Auto-tuned models are required to describe and follow changes in the degradation process and to describe the process and measurement noise.

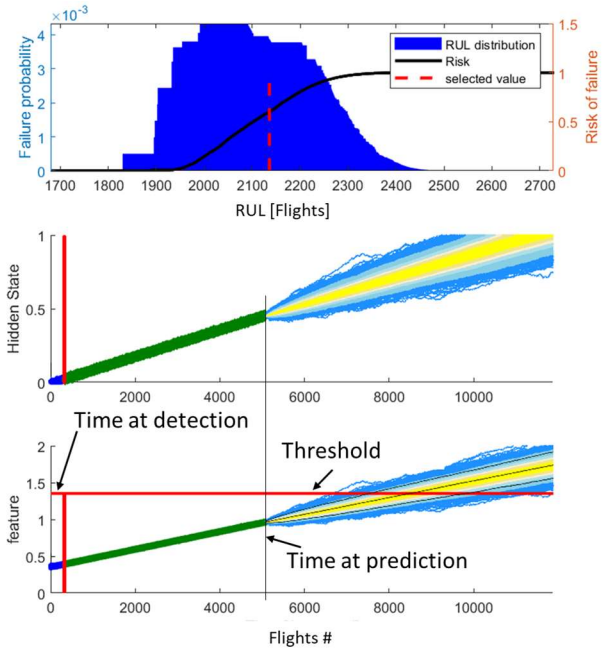

Figure 10. Prognostic output of the particle filtering framework for feature f_1.

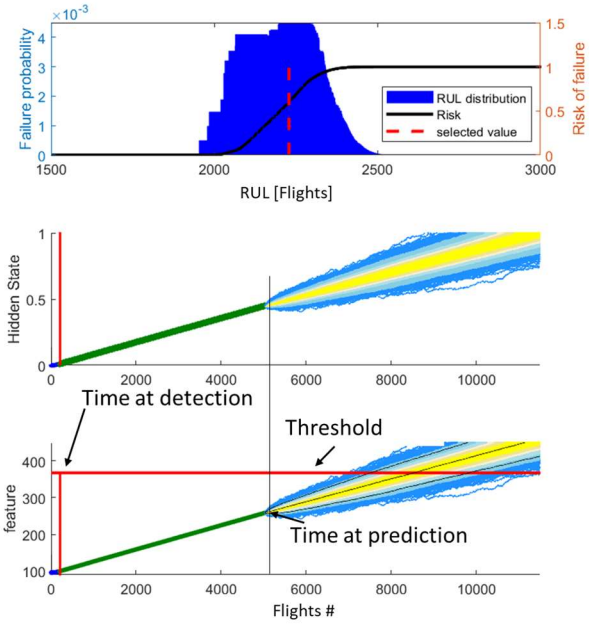

Figure 11. Prognostic output of the particle filtering framework for feature f_2.

An example of the results, comparing the behavior of the same algorithm applied to the two feature candidates f_1, and

f_2, are depicted in Figures 10 and 11, considering the same time at prediction. This example shows anecdotal evidence, further supported by the performance analysis provided in the next part of the paper, of the more accurate predictions provided by the feature f_2. The prognostic outputs were then analyzed through metrics traditionally employed in the preliminary analysis of PHM systems like the mean relative accuracy (RA) and the definition of a prognostic horizon (PH) associated with a certain relative accuracy threshold (Saxena et al. 2008). Although more rigorous metrics can be found in literature, mainly assessing the capability of the prognostic routine of estimating the probability distribution of the real Remaining Useful Life of the component, the presented study is focused on a first assessment of the feasibility and the benefit of a prognostic system for this particular application and not on the research for a new, more accurate technique for prognosis, which is planned for later stages of the research program. The $\alpha - \lambda$ diagram for the less favorable degradation history is provided Figure 12 for both features, highlighting the convergence of the RUL prediction towards the ground-truth and a stable accuracy level. In the considered case, the Prognostic Horizon accounts for the 68.7% of the projected operative life of the pads for the predictions performed with f_1, raising to more than 77.5% for analysis provided through the second feature f_2. The average RA during the performed simulations is above 80% in both cases.

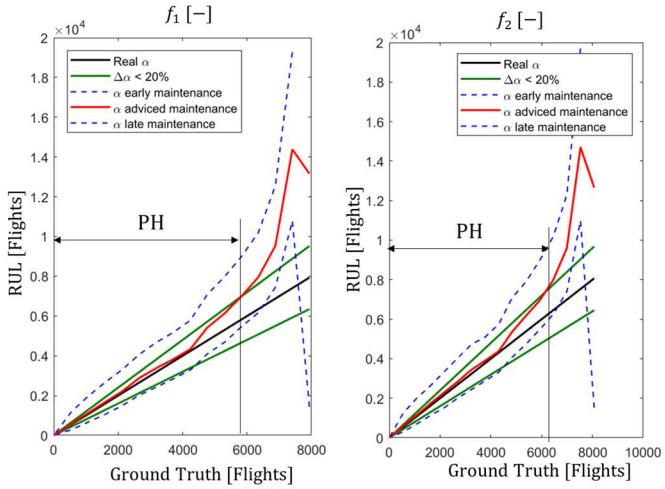

Figure 12. $\alpha - \lambda$ diagrams of long-term predictions obtained for features f_1 and f_2.

7. Conclusions

One of the main aims of the E-Lisa project is to propose the definition of a novel PHM system for Electro-mechanical brakes for aeronautic applications, which are expected to progressively replace the use of traditional hydraulic systems in aeronautic applications. Wear of the brake pads was assessed as one of the most significant failure modes, since it is inevitable during operations. Moreover, it naturally tends to evolve gradually in time, thus representing a favorable case-study for prognostic applications. To pursue this objective a high-fidelity model of the aircraft, of the landing gear leg and of the E-Brake system was prepare and presented. The model is able to reproduce an entire landing process and incorporate a dynamic degradation model, which simulate wear progression as a function of the simulated operations. Such model was used to generate data necessary to study the main macroscopic symptoms of wear progression and provide the basis for the feature selection process. A few feature candidates have been presented, and their performances evaluated according to traditional metrics. Finally, a fault detection/prognostic algorithm based on a combination of data driven and particle filtering techniques was presented and applied to the simulated datasets. Early results are encouraging, showing the system capability to detect the wear process at its onset and achieving good performance marks for long-term prognosis. Although promising, results shown in this paper are still preliminary and further evaluations are needed. Further work will be in particular addressed at investigating other major failure modes possibly affecting the E-Brake assembly, the impact of such failure modes on the selected features, as well as the definition of a complete Fault Detection and Identification routine.

Acknowledgments

The research work presented in this paper was performed within the E-Lisa project, which has received funding from the Clean Sky 2 Joint Undertaking under the European Union's Horizon 2020 research and innovation programme under grant agreement number 887222.

References

Acuña, D. E., and Orchard, M. E. (2017). "Particle-filtering-based failure prognosis via sigma-points: Application to Lithium-Ion battery State-of-Charge monitoring." *Mechanical Systems and Signal Processing*.

Acuña, D. E., and Orchard, M. E. (2018). "A theoretically rigorous approach to failure prognosis." *Proceedings of the 10th Annual Conference of the Prognostics and Health Management Society 2018 (PHM18), Philadelphia, PA, September 24-27*.

Arulampalam, M. S., Maskell, S., Gordon, N., and Clapp, T. (2009). "A Tutorial on Particle Filters for Online Nonlinear/NonGaussian Bayesian Tracking." *Bayesian Bounds for Parameter Estimation and Nonlinear Filtering/Tracking*, IEEE.

Autin, S., De Martin, A., Jacazio, G., Socheleau, J., and Vachtsevanos, G. J. (2021). "Results of a feasibility study of a Prognostic System for Electro-Hydraulic Flight Control Actuators." *International Journal of Prognostics and Health Management*, 12(3), 1–18.

Carbone, G., and Putignano, C. (2013). "A novel methodology to predict sliding and rolling friction of viscoelastic materials: Theory and experiments." *Journal of the Mechanics and Physics of Solids*, Elsevier, 61(8), 1822–1834.

Cook, M. (2012). *Flight dynamics principles: a linear systems approach to aircraft stability and control*. Butterworth-Heinemann.

M. Burckhardt. (1993). "Radschlupf-Regelsysteme." *Fahrwerktechnik: Würzburg: Vogel Verlag.*

De Martin, A., Jacazio, G., and Sorli, M. (2018). "Enhanced Particle Filter framework for improved prognosis of electro-mechanical flight controls actuators." *PHM Society European Conference, PHME 2018, Utrecht, Netherlands, July 3-6*.

De Martin, A., Jacazio, G., and Sorli, M. (2022). "Simulation of Runway Irregularities in a Novel Test Rig for Fully Electrical Landing Gear Systems." *Aerospace*, 9(2), 114.

De Martin, A., Jacazio, G., and Vachtsevanos, G. (2017). "Windings fault detection and prognosis in electro-mechanical flight control actuators operating in active-active configuration." *International Journal of Prognostics and Health Management*, 8(2).

Mohan, N., Undeland T.M., and Robbins, W. P. (2005). *Power Electronics*. John Wiley and Sons, Inc.

Oikonomou, A., Eleftheroglou, N., Freeman, F., Loutas, T., and Zarouchas, D. (2022). "Remaining Useful Life Prognosis of Aircraft Brakes." *International Journal of Prognostics and Health Management*, 13(1), 1–11.

Olesiak, Z., Pyryev, Y., and Yevtushenko, A. (1997). "Determination of temperature and wear during braking." *Wear*, 210(1–2), 120–126.

Orchard, M. E., and Vachtsevanos, G. J. (2009). "A particle-filtering approach for on-line fault diagnosis and failure prognosis." *Transactions of the Institute of Measurement and Control*.

Ramesh, G., Garza, P., and Perinpanayagam, S. (2021). "Digital simulation and identification of faults with neural network reasoners in brushed actuators employed in an e-brake system." *Applied Sciences (Switzerland)*, 11(19).

Roemer, M. J., Byington, C. S., Kacprzynski, G. J., Vachtsevanos, G., and Goebel, K. (2011). "Prognostics." *System Health Management: With Aerospace Applications*.

Saxena, A., Celaya, J., Balaban, E., Goebel, K., Saha, B., Saha, S., and Schwabacher, M. (2008). "Metrics for evaluating performance of prognostic techniques." *2008 International Conference on Prognostics and Health Management*, IEEE, Denver, CO, 1–17.

Vachtsevanos, G., Lewis, F., Roemer, M., Hess, A., and Wu, B. (2006). *Intelligent Fault Diagnosis and Prognosis for Engineering Systems*. *Intelligent Fault Diagnosis and Prognosis for Engineering Systems*, John Wiley & Sons, Inc., Hoboken, NJ, USA.

Yevtushenko, A., Kuciej, M., and Topczewska, K. (2017). "Analytical model for investigation of the effect of friction power on temperature in the disk brake." *Advances in Mechanical Engineering*, 9(12), 1–12.